Wave interaction with multiple adjacent floating solar panels with arbitrary constraints

Yifeng Yang (杨毅锋) ⬥ ; Kang Ren (任康) ⬥ ; Binzhen Zhou (周斌珍) ⬥ ; Shi Yan Sun (孙士艳) ✉ ⬥ ;
Luofeng Huang (黄洛枫) ⬥

Check for updates

CrossMark

View
Online

Export
Citation

Physics of Fluids

Special Topic:
Flow and Civil Structures

Submit Today

AIP Publishing

AIP Publishing

Wave interaction with multiple adjacent floating solar panels with arbitrary constraints

View Online   Export Citation   CrossMark

Yifeng Yang (杨毅锋),[1,2] (iD) Kang Ren (任康),[1] (iD) Binzhen Zhou (周斌珍),[3] (iD) Shi Yan Sun (孙士艳),[4,a] (iD)
and Luofeng Huang (黄洛枫)[2] (iD)

AFFILIATIONS

[1]Department of Mechanical Engineering, University College London, Torrington Place, London WC1E 7JE, United Kingdom
[2]School of Water, Energy and Environment, Cranfield University, Cranfield MK43 0AL, United Kingdom
[3]School of Civil Engineering and Transportation, South China University of Technology, Guangzhou 510641, China
[4]School of Naval Architecture & Ocean Engineering, Jiangsu University of Science and Technology, Zhenjiang 212003, China

[a]Author to whom correspondence should be addressed: shiyan_sun@just.edu.cn

ABSTRACT

The problem of wave interaction with multiple adjacent floating solar panels with arbitrary types and numbers of constraints is considered. All the solar panels are assumed to be homogeneous, with the same physical properties, as well as modeled by using the Kirchhoff-Love plate theory. The motion of the fluid is described by the linear velocity potential theory. The domain decomposition method is employed to obtain the solutions. In particular, the entire fluid domain is divided into two types, the one below the free surface, and the other below elastic plates. The velocity potential in the free surface domain is expressed into a series of eigenfunctions. By contrast, the boundary integral equation and the Green function are employed to construct the velocity potential of fluid beneath the entire elastic cover, with unknowns distributed along two interfaces and jumps of physical parameters of the plates. All these unknowns are solved from the system of linear equations, which is established from the matching conditions of velocity potentials and edge conditions. This approach is confirmed with much higher computational efficiency compared with the one only involving eigenfunction expansion for the fluid beneath each plate. Extensive results and discussions are provided for the reflection and transmission coefficients of water waves, maximum deflection, and principal strain of the elastic plates; especially, the influence of different types and numbers of edge constraints are investigated in detail.

Published under an exclusive license by AIP Publishing. https://doi.org/10.1063/5.0198106

I. INTRODUCTION

In recent years, photovoltaic (PV), commonly referred to as the solar panel, has emerged as one of the most economically viable renewable energy technologies in history.[1] Typically, the deployment of solar panels necessitates vast expanses of land to generate a substantial amount of electricity. However, this can pose challenges in regions where land resources are limited. Furthermore, there is also significant competition for land that serves multiple purposes, including agriculture for food production and conservation efforts to protect biodiversity. Consequently, a pivotal consideration arises regarding the optimal placement of these solar panels.[2] One of the solutions is to deploy floating solar panels at seas.[3] However, ocean waves may pose a substantial challenge to the effective operation of solar panels. On the one hand, the wave-induced motions of floating solar panels may adversely impact their energy efficiency. On the other hand, large movements or deformation caused by waves may carry the risk of structural damage,

resulting in significant economic losses. Therefore, it is necessary to investigate the hydrodynamic properties of floating solar panels in ocean waves.

Research based on linear theories has been well applied to hydroelasticity, such as sea-ice dynamics and wave-ice-structure interactions, where the linearized velocity potential theory is employed to describe the motion of fluid, and the ice sheet is modeled as a thin elastic plate. In particular, Fox and Squire[4] studied wave transmission and reflection by a semi-infinite floating ice sheet through the method of matched eigenfunction expansions (MEEs), where the edge of the sheet was assumed to be free to move. Later, a similar problem was considered by Balmforth and Craster,[5] where the Timoshenko–Mindlin equation was adopted to describe the ice sheet, and the Wiener–Hopf technique was used to derive the solution. Meylan and Squire[6] proposed an approximated solution based on an analytical solution of a semi-infinite ice sheet.[4] Wu *et al.*[7] studied the same problem and solved it exactly through MEE.

07 March 2024 13:22:56

For multiple floating ice plates, Sturova[8] studied the water wave diffraction by a semi-infinite composite elastic plate, which was modeled as a combination of two ice sheets of different properties, where one is of finite size and the other is semi-infinite. Evans and Porter[9] considered the problem of wave diffraction by an ice sheet fully covering the water surface with a narrow crack of infinite extent, where the free edge conditions were imposed at the crack. In their work, MEE and Green function methods were both employed to derive the solution. Williams and Squire[10] investigated the wave scattering by three floating ice sheets of different properties based on the method of Wiener–Hopf technique and residue calculus. The works mentioned above pertain to plates that are either interconnected or separated by minimal gaps. However, there are instances where the spacing between two plates may be obvious. For example, Chung and Fox[11] studied the reflection and transmission of waves across a gap between two semi-infinite ice sheets. Shi et al.[12] studied the problem of wave diffraction by multiple wide-space ice sheets approximately. Furthermore, if offshore structures such as ships working in polar regions, the effects of structures should be further considered. Typically, Ren et al.[13] considered the wave-excited motions of a body floating on water confined between two semi-infinite ice sheets, where the fluid domain was divided into several sub-regions, and the MEE was applied to match the solution at each interface.

The thin elastic plate model and linearized velocity potential theory were also used to study the interaction between water waves and floating offshore structures. For example, Karmakar and Soares[14] derived an analytical solution for a floating elastic plate with two edges moored to the seabed based on MEE, where the mooring lines were modeled as springs to provide extra vertical reaction. Mohapatra et al.[15] considered the problem of wave diffraction by a finite floating elastic plate with an inner compressible force. Karmakar et al.[16] solved the problem of wave interaction with multiple articulated floating elastic plates fully covering the entire free surface by using MEE. Later, Praveen et al.[17] further extended it to plates of finite size. A more recent work by Zhang et al.[18] studied the hydroelastic response of two floating photovoltaic structures over stepped seabed condition.

As discussed above, a considerable volume of studies has been conducted to investigate the hydrodynamic properties of floating elastic structures. In the context of floating solar panels at sea, it is observed that their hydrodynamic performance does exhibit certain similarities with ice sheets. For instance, when an ice sheet or a group of floating solar panels covers a large amount of free surface region, the structural elasticity in both cases is quite important. Nonetheless, the hydrodynamic problems for ice sheets and floating solar panels also show discernible differences. For example, ice sheets inherently exist in nature, and it is common to assume that the edge of sea ice is free to move.[19] By contrast, solar panels are human-made, and their edge conditions are much more complicated, which should be determined based on the connections between each two adjacent panels, as well as the mooring lines used in the structure. In addition, ice sheets are normally shown in nature with diverse physical properties[20] (e.g., thickness). By contrast, one floating solar farm usually consists of solar panels with identical properties. These distinct differences suggest that the solution procedure developed for issues involving ice sheets may not be entirely suitable and efficient to solve problems of floating solar panels. In particular, when addressing problems involving ice sheets of

different properties, a conventional approach is to treat the fluid beneath each ice sheet as a subdomain, and the velocity potential in each subdomain is written into a series of eigenfunctions with unknown coefficients. Subsequently, the velocity potential can be matched at each interface by using MEE to solve these unknowns, a typical example is given by Ren et al.[13] Although this approach has demonstrated considerable efficacy in numerous applications, it may not be so numerically efficient for the current floating panels problem we considered in this work. In the case of the floating solar panels, the problem will be highly computationally demanding if we choose to follow the regular procedure above to expand the velocity potential into a series of eigenfunctions in each subdomain, especially when the numbers of panels and constraints are large or even huge. Therefore, we develop an alternative and more efficient scheme for floating solar panels, featured by the combination of the Green function technique and MEE. In this scheme, by modeling each floating solar panel as a thin elastic plate with identical and homogeneous properties, the velocity potential beneath the entire floating solar panels can be constructed from the boundary integral equation. Through using the Green function corresponding to fluid fully covered by a homogeneous elastic plate, only line integrals along two interfaces of the free surface and elastic covers, as well as the jumps at the edges of the plates need to be remained in the boundary integration equation. In such a case, unknowns only need to be distributed on the velocity potential on two interfaces and jumps at the edges of elastic plates. Compared with the conventional MEE procedure,[13] the total number of unknowns is significantly reduced. Moreover, the addition of one more plate to the system only leads to an increment in unknowns at the newly introduced edge, which significantly improves the computational efficiency, especially for a floating solar farm with a significant number of panels. Based on the present procedure, case studies are conducted for three typical edge conditions, namely, pinned, hinged, and free. The effects of edge conditions on the reflected and transmitted waves, as well as the hydroelastic response of the floating solar panels, are investigated in detail.

The work is organized as follows: The mathematical model or governing equation and boundary conditions of the problem are formulated in Sec. II. In Sec. III, the solution procedure is presented. Then, the results and discussions are made in Sec. IV. Finally, conclusions are drawn in Sec. V.

II. MATHEMATICAL MODEL

In this study, we examine a floating solar farm covering a large horizontal area of open water. Like many water wave-related problems, we simplify the analysis by considering a two-dimensional scenario, as illustrated in Fig. 1. In contrast, when the transverse dimension of the structure or fluid environment is significant to the problem, the three-dimensional effect is important to be considered (see Yang et al.[21] and Ren et al.[22]). A Cartesian coordinate system O-xz is introduced, with the x-axis along the clam water surface and the z-axis pointing upward. The seabed is located horizontally along $z = -H$. The water surface region $-d \le x \le d$ is covered by multiple floating elastic plates with homogeneous properties. The density and thickness of the plate are ρ_e and h_e, respectively. In addition to two side edges at $x = \pm d$, there are also internal constraints between each two adjacent elastic panels. In particular, the internal pins are applied at $x = a_i$ ($i = 1 \sim N_a$) with $a_i < a_{i+1}$, two sides of the plate are hinged to each other at $x = b_i$ ($i = 1 \sim N_b$) with $b_i < b_{i+1}$, as well as two sides of the
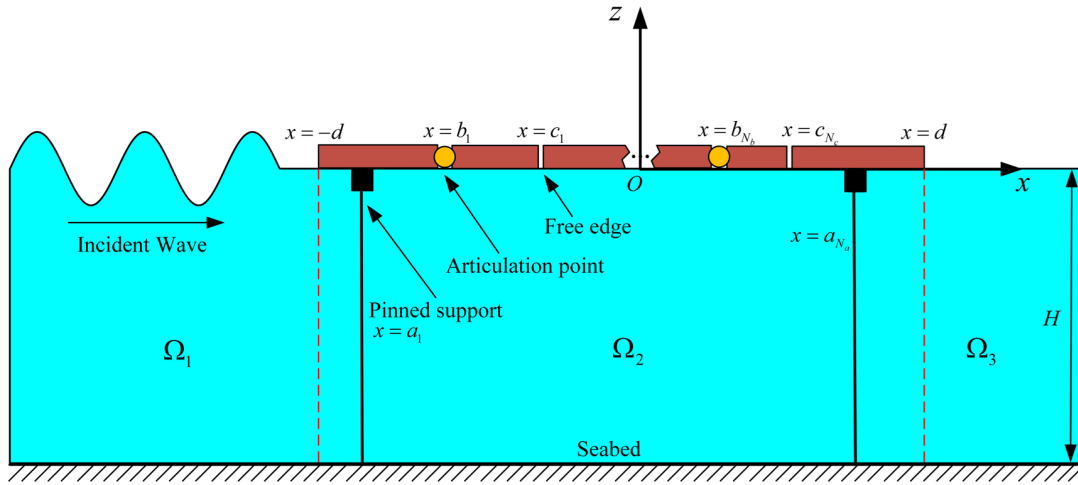
FIG. 1. The sketch of an incident wave interaction with a floating elastic plate.

TABLE I. Positions of different types of internal constraints of the floating solar panels.

Edge type	Position
Pinned	$x = a_1, a_2, \ldots, a_{N_a}$
Hinged	$x = b_1, b_2, \ldots, b_{N_b}$
Free	$x = c_1, c_2, \ldots, c_{N_c}$

plate are free to each other at $x = c_i$ ($i = 1 \sim N_c$) with $c_i < c_{i+1}$, as given in Table I. An incoming wave comes from $x = -\infty$ to $x = +\infty$ and will interact with the entire floating solar panels.

The fluid with density ρ is assumed to be homogeneous, inviscid, incompressible, and its motion is irrotational. Under the further assumption made on the small-amplitude motion of the wave, the linearized velocity potential theory is used to describe the flow. Once the motion is sinusoidal in time t with radian frequency ω, the total velocity potential can be written as

$$\Phi(x, z, t) = \text{Re}\{\phi(x, z)e^{i\omega t}\}, \quad (1)$$

where the spatial velocity potential $\phi(x,z)$ contains the incident component $\phi_I(x,z)$ and the diffracted component $\phi_D(x,z)$. $\phi(x,z)$ is governed by the Laplace equation in the fluid domain, which can be written as

$$\frac{\partial^2 \phi}{\partial x^2} + \frac{\partial^2 \phi}{\partial z^2} = 0. \quad (2)$$

The linearized boundary condition on the free surface region can be expressed as

$$\frac{\partial \phi}{\partial z} - \frac{\omega^2}{g}\phi = 0, \quad |x| > d, \, z = 0, \quad (3)$$

where g denotes the acceleration due to gravity. The boundary condition on the floating elastic plate gives

$$\left(L\frac{\partial^4}{\partial x^4} - m_e\omega^2 + \rho g\right)\frac{\partial \phi}{\partial z} - \rho\omega^2\phi = 0, \quad |x| < d, \, z = 0, \quad (4)$$

where $L = \frac{Eh_e^3}{12(1-\nu^2)}$ represents the effective flexural rigidity of the elastic plate; E and ν denote Young's modulus and Poisson's ratio, respectively; and $m_e = \rho_e h_e$ is the mass per unit area of the plate. In Eq. (4), following the previous assumptions on elastic plates,[16,23] the structural damping of the plate has not been considered. When doing so, an extra damping term may need to be involved in Eq. (4), and the Green function used in the current scheme may need to be re-derived.

On the flat seabed, the impermeable boundary condition should be enforced as

$$\frac{\partial \phi}{\partial z} = 0, \quad z = -H. \quad (5)$$

At the side edges of the entire system of floating elastic plates, two different conditions are considered, namely, the free edge and pinned edge conditions. The free edge conditions require zero Kirchhoff's shear force and bending moment. The pinned edge conditions require zero deflection and bending moment, which can be used to model the edge of the plate is completely moored to the seabed. Based on the above discussion, we have

$$\begin{cases} \dfrac{\partial^3 \phi}{\partial x^2 \partial z} = 0, \, \dfrac{\partial^4 \phi}{\partial x^3 \partial z} = 0 & \text{Free edge,} \quad (6a) \\ \dfrac{\partial \phi}{\partial z} = 0, \, \dfrac{\partial^3 \phi}{\partial x^2 \partial z} = 0 & \text{Pinned edge,} \quad (6b) \end{cases}$$

where $x = -d^+$ and $x = d^-$, $z = 0$.

In addition to the conditions at two side edges of the plates, edge conditions may also be applied to the internal constraints. The internal pins are used to model extra moored points of the elastic plate in addition to these at two sides, where the deflection is zero, the slope and bending moment are continuous, or

$$\left(\frac{\partial \phi}{\partial z}\right)_{x=a_i} = 0, \tag{7a}$$

$$\left(\frac{\partial^2 \phi}{\partial x \partial z}\right)_{x=a_i^-} = \left(\frac{\partial^2 \phi}{\partial x \partial z}\right)_{x=a_i^+}, \tag{7b}$$

$$\left(\frac{\partial^3 \phi}{\partial x^2 \partial z}\right)_{x=a_i^-} = \left(\frac{\partial^3 \phi}{\partial x^2 \partial z}\right)_{x=a_i^+}, \tag{7c}$$

where $i = 1 \sim N_a$.

At the location when two sides of the plate are hinged to each other, the bending moment here should be zero, as well as the deflection and shear force are continuous, or

$$\left(\frac{\partial \phi}{\partial z}\right)_{x=b_i^-} = \left(\frac{\partial \phi}{\partial z}\right)_{x=b_i^+}, \tag{8a}$$

$$\left(\frac{\partial^3 \phi}{\partial x^2 \partial z}\right)_{x=b_i} = 0, \tag{8b}$$

$$\left(\frac{\partial^4 \phi}{\partial x^3 \partial z}\right)_{x=b_i^-} = \left(\frac{\partial^4 \phi}{\partial x^3 \partial z}\right)_{x=b_i^+}, \tag{8c}$$

where $i = 1 \sim N_b$.

For internal free edges, we have

$$\left(\frac{\partial^3 \phi}{\partial x^2 \partial z}\right)_{x=c_i} = 0, \tag{9a}$$

$$\left(\frac{\partial^4 \phi}{\partial x^3 \partial z}\right)_{x=c_i} = 0, \tag{9b}$$

where $i = 1 \sim N_c$.

The far-field radiation conditions should be imposed at infinity to ensure wave propagating outwards, which gives

$$\lim_{x \to \pm\infty} \left(\frac{\partial \phi_D}{\partial x} \pm i\mathcal{k}_0 \phi_D\right) = 0, \tag{10}$$

where $\mathcal{k}_0$ is the wavenumber of the propagation wave, which will be discussed later.

III. SOLUTION PROCEDURE

The method of domain decomposition is used to derive the solution. As discussed in Sec. II, there is a total of $N_a + N_b + N_c + 2$ edges in the floating solar panels shown in Fig. 1. The entire fluid domain here is only divided into three parts, where two subdomains with the free surface or Ω_1 ($-\infty < x < -d$, $-H \le z \le 0$) and Ω_3 ($d < x < +\infty$, $-H \le z \le 0$), as well as the subdomain below the entire elastic plates or Ω_2 ($-d \le x \le d$, $-H \le z \le 0$). The velocity potential in each subdomain Ω_i ($i = 1, 2, 3$) is denoted as $\phi^{(i)}$. $\phi^{(1)}$ and $\phi^{(3)}$ can be expanded into a series of eigenfunctions, while $\phi^{(2)}$ can be constructed by using the boundary integral equation.

Based on the above discussion, $\phi^{(1)}$ may be written as

$$\phi^{(1)}(x, z) = \phi_I(x, z) + \phi_D^{(1)}(x, z), \tag{11}$$

where the incident velocity potential $\phi_I(x, z)$ can be expressed as

$$\phi_I(x, z) = I\varphi_0(z)e^{-i\mathcal{k}_0 x}, \tag{12}$$

where $I = -i\frac{Ag}{\omega}$, A denotes the amplitude of the incident wave, $\mathcal{k}_0$ denotes the wave number along the x direction, and $\varphi_0(z)$ is a mode function corresponding to $\mathcal{k}_0$. Based on the far-field radiation condition Eq. (10), $\phi_D^{(1)}(x, z)$ can be expanded in the following series form as:

$$\phi_D^{(1)}(x, z) = \sum_{m=0}^{+\infty} A_m \varphi_m(z) e^{i\mathcal{k}_m x}, \tag{13}$$

where A_m ($m = 0, 1, 2\ldots$) are unknown coefficients, as well as

$$\varphi_m(z) = \frac{\cosh \mathcal{k}_m(z + H)}{\cosh \mathcal{k}_m H}, \quad m = 0, 1, 2\ldots, \tag{14}$$

with $\mathcal{k}_m$ satisfy the following dispersion equation of free surface wave:

$$K_1(\mathcal{k}_m, \omega) \equiv \mathcal{k}_m \tanh \mathcal{k}_m - \frac{\omega^2}{g} = 0. \tag{15}$$

Here, $\mathcal{k}_0$ is the positive real root, and $\mathcal{k}_m$ ($m = 1, 2, 3\ldots$) are an infinite number of purely negative imaginary roots.

The velocity potential $\phi^{(3)}$ in Ω_3 can be also treated in this way, which provides

$$\phi^{(3)}(x, z) = \sum_{m=0}^{+\infty} B_m \varphi_m(z) e^{-i\mathcal{k}_m x}, \tag{16}$$

where B_m ($m = 0, 1, 2\ldots$) are unknown coefficients. Due to the internal constraints in the floating elastic plates, the velocity potential $\phi^{(2)}$ in Ω_2 cannot simply be written as a series of eigenfunctions. Alternatively, we may use the Green function method to construct $\phi^{(2)}$ here. To do that, the Green function G corresponding to the water surface fully covered by a homogeneous elastic plate is first introduced[24]

$$G(x, z; x_0, z_0)$$
$$= \ln\left(\frac{r_1}{H}\right) + \ln\left(\frac{r_2}{H}\right)$$
$$- 2\int_0^{+\infty} \frac{e^{-\alpha H}}{\alpha} \left[\frac{P(\alpha)Z(\alpha, z)Z(\alpha, z_0)\cos\alpha(x - x_0)}{K_2(\alpha, \omega)Z(\alpha, 0)} + 1\right] d\alpha, \tag{17}$$

where

$$P(\alpha) = \left(L\alpha^4 + \rho g - m_e\omega^2\right)\alpha + \rho\omega^2, \tag{18a}$$

$$K_2(\alpha, \omega) = \left(L\alpha^4 + \rho g - m_e\omega^2\right)\alpha \sinh\alpha H - \rho\omega^2\cosh\alpha H \tag{18b}$$

$$Z(\alpha, z) = \cosh\alpha(z + H). \tag{18c}$$

r_1 is the distance between the field point (x, z) and source point (x_0, z_0), and r_2 is the distance between the field point (x, z) and point $(x_0, -z_0 - 2H)$. G in Eq. (17) can be also converted into a series form, we may first extend the integral range from $(0, +\infty)$ to $(-\infty, +\infty)$, and then apply the theorem of residue, through some algebra, we have

$$G(x, z; x_0, z_0) = \pi i \sum_{m=-2}^{+\infty} \frac{\psi_m(z)\psi_m(z_0)}{\kappa_m Q_m} e^{-i\kappa_m|x-x_0|}, \tag{19}$$

where

$$Q_m = \frac{2\kappa_m H + \sinh(2\kappa_m H)}{4\kappa_m \cosh^2(\kappa_m H)} + \frac{2L\kappa_m^4}{\rho\omega^2}\tanh^2(\kappa_m H), \tag{20}$$

$$\psi_m(z) = \frac{\cosh\kappa_m(z+H)}{\cosh\kappa_m H}, \quad m = -2, -1, 0\ldots \tag{21}$$

κ_m are the roots of the dispersion equation corresponding to the fluid fully covered by an elastic plate, or $K_2(\kappa_m, \omega) = 0$. κ_{-2} and κ_{-1} are two fully complex roots with negative imaginary parts and satisfy $\bar{\kappa}_{-1} = -\kappa_{-2}$, κ_0 is the purely positive real root, κ_m ($m = 1, 2, 3\ldots$) are an infinite number of purely negative imaginary roots.

As G is symmetrical about coordinates (x, z) and (x_0, z_0), we may exchange (x, z) with (x_0, z_0) below. Applying the Green's second identity, $\phi^{(2)}(x, z)$ can be written as

$$2\pi\phi^{(2)}(x, z) = \oint_{\mathcal{L}} \left[\phi^{(2)}(x_0, z_0)\frac{\partial G(x, z; x_0, z_0)}{\partial n_0} - G(x, z; x_0, z_0)\frac{\partial\phi^{(2)}(x_0, z_0)}{\partial n_0}\right]ds_0, \tag{22}$$

where $\mathcal{L}$ is comprised of lines $x_0 = -d$, $z_0 = 0$, $x_0 = d$, and $z_0 = -H$, $\partial/\partial n_0$ denotes the normal derivative with respect to (x_0, z_0) along $\mathcal{L}$. Since both G and $\phi^{(2)}$ satisfy the boundary conditions on the seabed, Eq. (22) can be further written as

$$2\pi\phi^{(2)}(x, z) = \left\{\begin{array}{l} \displaystyle\int_{-d}^{d}\left[\phi^{(2)}(x_0, 0)\frac{\partial G(x, z; x_0, 0)}{\partial z_0} - G(x, z; x_0, 0)\frac{\partial\phi^{(2)}(x_0, 0)}{\partial z_0}\right]dx_0 \\[2ex] \displaystyle-\int_{-H}^{0}\left[\phi^{(2)}(-d, z_0)\frac{\partial G(x, z; -d, z_0)}{\partial x_0} - G(x, z; -d, z_0)\frac{\partial\phi^{(2)}(-d, z_0)}{\partial x_0}\right]dz_0 \\[2ex] \displaystyle+\int_{-H}^{0}\left[\phi^{(2)}(d, z_0)\frac{\partial G(x, z; d, z_0)}{\partial x_0} - G(x, z; d, z_0)\frac{\partial\phi^{(2)}(d, z_0)}{\partial x_0}\right]dz_0 \end{array}\right\}. \tag{23}$$

Applying the boundary condition on the elastic plate in Eq. (4) to the first integral on the right-hand side of Eq. (23), as well as using integration by parts, as in Yang *et al.*,[21] we obtain

$$\int_{-d}^{d}\left[\phi^{(2)}(x_0, 0)\frac{\partial G(x, z; x_0, 0)}{\partial z_0} - G(x, z; x_0, 0)\frac{\partial\phi^{(2)}(x_0, 0)}{\partial z_0}\right]dx_0$$

$$= \frac{L}{\rho\omega^2}\left\{\begin{array}{l} \displaystyle\sum_{i=1}^{N_a}\left(\frac{\partial^4\phi^{(2)}}{\partial x_0^3\partial z_0}\frac{\partial G}{\partial z_0} - \frac{\partial^4 G}{\partial x_0^3\partial z_0}\frac{\partial\phi^{(2)}}{\partial z_0} - \frac{\partial^3\phi^{(2)}}{\partial x_0^2\partial z_0}\frac{\partial^2 G}{\partial x_0\partial z_0} + \frac{\partial^3 G}{\partial x_0^2\partial z_0}\frac{\partial^2\phi^{(2)}}{\partial x_0\partial z_0}\right)_{x_0=a_i^+}^{x_0=a_i^-} \\[3ex] \displaystyle+\sum_{i=1}^{N_b}\left(\frac{\partial^4\phi^{(2)}}{\partial x_0^3\partial z_0}\frac{\partial G}{\partial z_0} - \frac{\partial^4 G}{\partial x_0^3\partial z_0}\frac{\partial\phi^{(2)}}{\partial z_0} - \frac{\partial^3\phi^{(2)}}{\partial x_0^2\partial z_0}\frac{\partial^2 G}{\partial x_0\partial z_0} + \frac{\partial^3 G}{\partial x_0^2\partial z_0}\frac{\partial^2\phi^{(2)}}{\partial x_0\partial z_0}\right)_{x_0=b_i^+}^{x_0=b_i^-} \\[3ex] \displaystyle+\sum_{i=1}^{N_c}\left(\frac{\partial^4\phi^{(2)}}{\partial x_0^3\partial z_0}\frac{\partial G}{\partial z_0} - \frac{\partial^4 G}{\partial x_0^3\partial z_0}\frac{\partial\phi^{(2)}}{\partial z_0} - \frac{\partial^3\phi^{(2)}}{\partial x_0^2\partial z_0}\frac{\partial^2 G}{\partial x_0\partial z_0} + \frac{\partial^3 G}{\partial x_0^2\partial z_0}\frac{\partial^2\phi^{(2)}}{\partial x_0\partial z_0}\right)_{x_0=c_i^+}^{x_0=c_i^-} \\[3ex] \displaystyle+\left(\frac{\partial^4\phi^{(2)}}{\partial x_0^3\partial z_0}\frac{\partial G}{\partial z_0} - \frac{\partial^4 G}{\partial x_0^3\partial z_0}\frac{\partial\phi^{(2)}}{\partial z_0} - \frac{\partial^3\phi^{(2)}}{\partial x_0^2\partial z_0}\frac{\partial^2 G}{\partial x_0\partial z_0} + \frac{\partial^3 G}{\partial x_0^2\partial z_0}\frac{\partial^2\phi^{(2)}}{\partial x_0\partial z_0}\right)_{x_0=-d}^{x_0=d} \end{array}\right\}_{z_0=0}. \tag{24}$$

To simplify Eq. (24), we may invoke the conditions at the internal constraints. Using Eqs. (7)–(9), we have $\left(\frac{\partial\phi^{(2)}}{\partial z_0}\right)_{x_0=a_i^+}^{x_0=a_i^-} = \left(\frac{\partial^2\phi^{(2)}}{\partial x_0\partial z_0}\right)_{x_0=a_i^+}^{x_0=a_i^-}$ $= \left(\frac{\partial^3\phi^{(2)}}{\partial x_0^2\partial z_0}\right)_{x_0=a_i^+}^{x_0=a_i^-} = 0$, which means there is no jump in the deflection, slope and bending moment. $\left(\frac{\partial\phi^{(2)}}{\partial z_0}\right)_{x_0=b_i^+}^{x_0=b_i^-} = \left(\frac{\partial^3\phi^{(2)}}{\partial x_0^2\partial z_0}\right)_{x_0=b_i^+}^{x_0=b_i^-}$ $= \left(\frac{\partial^4\phi^{(2)}}{\partial x_0^3\partial z_0}\right)_{x_0=b_i^+}^{x_0=b_i^-} = 0$, which alludes no jump in the deflection, bending moment and shear force. In addition, $\left(\frac{\partial^4\phi^{(2)}}{\partial x_0^3\partial z_0}\right)_{x_0=c_i^+}^{x_0=c_i^-} = \left(\frac{\partial^3\phi^{(2)}}{\partial x_0^2\partial z_0}\right)_{x_0=c_i^+}^{x_0=c_i^-} = 0$. We may further define these jumps at a_i, b_i, and c_i as the following unknowns.

$$\begin{cases} \alpha_i = \frac{L}{2\pi\rho\omega^2} \left(\frac{\partial^4 \phi^{(2)}}{\partial x_0^3 \partial z_0} \right) \Big|_{x_0=a_i^+}^{x_0=a_i^-}, \quad i = 1 \sim N_a, & \text{(25a)} \\[3mm] \beta_i = \frac{L}{2\pi\rho\omega^2} \left(\frac{\partial^2 \phi^{(2)}}{\partial x_0 \partial z_0} \right) \Big|_{x_0=b_i^+}^{x_0=b_i^-}, \quad i = 1 \sim N_b, & \text{(25b)} \\[3mm] \gamma_i = \frac{L}{2\pi\rho\omega^2} \left(-\frac{\partial \phi^{(2)}}{\partial z_0} \right) \Big|_{x_0=c_i^+}^{x_0=c_i^-}, \quad \mu_i = \frac{L}{2\pi\rho\omega^2} \left(\frac{\partial^2 \phi^{(2)}}{\partial x_0 \partial z_0} \right) \Big|_{x_0=c_i^+}^{x_0=c_i^-}, \quad i = 1 \sim N_c, & \text{(25c)} \end{cases}$$

as well as introduce

$$\mathcal{G}(x,z,x_0) = \frac{\partial G(x,z;x_0;0)}{\partial z_0} = \pi i \sum_{m=-2}^{+\infty} \frac{\psi_m(z)\tanh(\kappa_m H)e^{-i\kappa_m|x-x_0|}}{Q_m}. \tag{26}$$

In Eq. (24), we may apply the Laplace equation, or $\frac{\partial^2}{\partial x_0^2} = -\frac{\partial^2}{\partial z_0^2}$ to the terms of G and $\phi^{(2)}$ at $x_0 = \pm d$. Together with the above discussion, Eq. (24) becomes

$$\int_{-d}^{d} \left[\phi^{(2)}(x_0,0) \frac{\partial G(x,z;x_0,0)}{\partial z_0} - G(x,z;x_0,0) \frac{\partial \phi^{(2)}(x_0,0)}{\partial z_0} \right] dx_0$$

$$= \begin{cases} 2\pi \sum_{i=1}^{N_a} \alpha_i \mathcal{G}(x,z,a_i) + 2\pi \sum_{i=1}^{N_b} \beta_i \frac{\partial^2 \mathcal{G}(x,z,b_i)}{\partial x_0^2} + 2\pi \sum_{i=1}^{N_c} \left[\gamma_i \frac{\partial^3 \mathcal{G}(x,z,c_i)}{\partial x_0^3} + \mu_i \frac{\partial^2 \mathcal{G}(x,z,c_i)}{\partial x_0^2} \right] \\[3mm] + \frac{L}{\rho\omega^2} \left(-\frac{\partial^4 \phi^{(2)}}{\partial x_0 \partial z_0^3} \frac{\partial G}{\partial z_0} + \frac{\partial^4 G}{\partial x_0 \partial z_0^3} \frac{\partial \phi^{(2)}}{\partial z_0} + \frac{\partial^3 \phi^{(2)}}{\partial z_0^3} \frac{\partial^2 G}{\partial x_0 \partial z_0} - \frac{\partial^3 G}{\partial z_0^3} \frac{\partial^2 \phi^{(2)}}{\partial x_0 \partial z_0} \right) \Big|_{x_0=-d}^{x_0=d} \end{cases}. \tag{27}$$

Substituting Eq. (27) into (23) and using the following inner product for z_0,[25]

$$\langle f,g \rangle = \int_{-H}^{0} fg\, dz_0 + \frac{L}{\rho\omega^2} \left(\frac{d^3 f}{dz^3} \frac{dg}{dz} + \frac{df}{dz} \frac{d^3 g}{dz^3} \right) \Big|_{z_0=0}. \tag{28}$$

We have

$$\phi^{(2)}(x,z) = \frac{1}{2\pi} \begin{cases} \left\langle \frac{\partial G(x,z;d,z_0)}{\partial x_0}, \phi^{(2)}(d,z_0) \right\rangle - \left\langle G(x,z;d,z_0), \frac{\partial \phi^{(2)}(d,z_0)}{\partial x_0} \right\rangle \\[3mm] + \left\langle G(x,z;-d,z_0), \frac{\partial \phi^{(2)}(-d,z_0)}{\partial x_0} \right\rangle - \left\langle \frac{\partial G(x,z;-d,z_0)}{\partial x_0}, \phi^{(2)}(-d,z_0) \right\rangle \end{cases}$$

$$+ \begin{cases} \sum_{i=1}^{N_a} \alpha_i \mathcal{G}(x,z,a_i) + \sum_{i=1}^{N_b} \beta_i \frac{\partial^2 \mathcal{G}(x,z,b_i)}{\partial x_0^2} \\[3mm] + \sum_{i=1}^{N_c} \left[\gamma_i \frac{\partial^3 \mathcal{G}(x,z,c_i)}{\partial x_0^3} + \mu_i \frac{\partial^2 \mathcal{G}(x,z,c_i)}{\partial x_0^2} \right] \end{cases}, \quad |x| < d. \tag{29}$$

Based on the derivation in Yang *et al.*,[26] the terms at $x_0 = \pm d$ in Eq. (29) are equivalent to be written via a source distribution formula, which gives

$$\phi^{(2)}(x,z) = \langle G(x,z;d,z_0), \Psi_+(z_0) \rangle - \langle G(x,z;-d,z_0), \Psi_-(z_0) \rangle + \begin{cases} \sum_{i=1}^{N_a} \alpha_i \mathcal{G}(x,z,a_i) + \sum_{i=1}^{N_b} \beta_i \frac{\partial^2 \mathcal{G}(x,z,b_i)}{\partial x_0^2} \\[3mm] + \sum_{i=1}^{N_c} \left[\gamma_i \frac{\partial^3 \mathcal{G}(x,z,c_i)}{\partial x_0^3} + \mu_i \frac{\partial^2 \mathcal{G}(x,z,c_i)}{\partial x_0^2} \right] \end{cases}, \quad |x| < d, \tag{30}$$

where $\Psi_\pm(z_0)$ are the source strengths along the lines $x_0 = \pm d$, respectively. We may expand $\Psi_\pm(z_0)$ as the following series of eigenfunctions:

$$
\begin{cases}
\Psi_+(z_0) = \dfrac{1}{\pi i} \displaystyle\sum_{m=-2}^{+\infty} \kappa_m e^{i\kappa_m d} C_m \psi_m(z), & \text{(31a)} \\[4mm]
\Psi_-(z_0) = \dfrac{1}{\pi i} \displaystyle\sum_{m=-2}^{+\infty} \kappa_m e^{i\kappa_m d} D_m \psi_m(z), & \text{(31b)}
\end{cases}
$$

where C_m and D_m are unknown coefficients. Substituting Eqs. (19) and (31) into Eq. (30), as well as invoking the orthogonality of inner product $\langle \psi_m(z_0), \psi_{\bar{m}}(z_0) \rangle = \delta_{m\bar{m}} Q_m$, where $\delta_{m\bar{m}}$ denotes the Kronecker delta function, which gives

$$
\phi^{(2)}(x,z) = \sum_{m=-2}^{+\infty} \left(C_m e^{-i\kappa_m x} + D_m e^{i\kappa_m x} \right) \psi_m(z) + \left\{ \begin{array}{l} \displaystyle\sum_{i=1}^{N_a} \alpha_i \mathcal{G}(x,z,a_i) + \sum_{i=1}^{N_b} \beta_i \dfrac{\partial^2 \mathcal{G}(x,z,b_i)}{\partial x_0^2} \\[4mm] + \displaystyle\sum_{i=1}^{N_c} \left[\gamma_i \dfrac{\partial^3 \mathcal{G}(x,z,c_i)}{\partial x_0^3} + \mu_i \dfrac{\partial^2 \mathcal{G}(x,z,c_i)}{\partial x_0^2} \right] \end{array} \right\}, \quad |x| < d. \tag{32}
$$

To solve the unknown coefficients A_m, B_m, C_m, D_m, α_i, β_i, γ_i, and μ_i, we may use the continuous conditions of the velocity potential and dynamic pressure at two interfaces $x = \pm d$, or

$$
\begin{cases}
\phi^{(1)}(-d^-, z) = \phi^{(2)}(-d^+, z), & \text{(33a)} \\[3mm]
\dfrac{\partial \phi^{(1)}(-d^-, z)}{\partial x} = \dfrac{\partial \phi^{(2)}(-d^+, z)}{\partial x}, & \text{(33b)} \\[3mm]
\phi^{(2)}(d^-, z) = \phi^{(3)}(d^+, z), & \text{(33c)} \\[3mm]
\dfrac{\partial \phi^{(2)}(d^-, z)}{\partial x} = \dfrac{\partial \phi^{(3)}(d^+, z)}{\partial x}. & \text{(33d)}
\end{cases}
$$

To match the velocity potentials at $x = \pm d$, from Eqs. (33a) and (33c), we have

$$
\begin{cases}
\displaystyle\int_{-H}^{0} \phi^{(1)}(-d, z) \varphi_m(z) dz = \int_{-H}^{0} \phi^{(2)}(-d, z) \varphi_m(z) dz, & \text{(34a)} \\[4mm]
\displaystyle\int_{-H}^{0} \phi^{(3)}(d, z) \varphi_m(z) dz = \int_{-H}^{0} \phi^{(2)}(d, z) \varphi_m(z) dz. & \text{(34b)}
\end{cases}
$$

Substituting Eqs. (11), (12), (13), (16), and (32) into Eqs. (34a) and (34b), as well as using the orthogonality of $\varphi_m(z)$, which gives the following system of linear equations:

$$
P_m e^{-i\mathscr{k}_m d} A_m - \sum_{m'=-2}^{+\infty} X(\kappa_{m'}, \mathscr{k}_m) \left(e^{i\kappa_{m'} d} C_{m'} + e^{-i\kappa_{m'} d} D_{m'} \right)
$$

$$
- \left\{ \begin{array}{l} \displaystyle\sum_{i=1}^{N_a} \mathcal{F}_m(-d, a_i) \alpha_i + \sum_{i=1}^{N_b} \dfrac{\partial^2 \mathcal{F}_m(-d, b_i)}{\partial x_0^2} \beta_i \\[4mm] + \displaystyle\sum_{i=1}^{N_c} \left[\dfrac{\partial^3 \mathcal{F}_m(-d, c_i)}{\partial x_0^3} \gamma_i + \dfrac{\partial^2 \mathcal{F}_m(-d, c_i)}{\partial x_0^2} \mu_i \right] \end{array} \right\} = -\delta_{m0} I P_0 e^{i\mathscr{k}_0 d}, \quad m = 0, 1, 2\ldots, \tag{35a}
$$

$$
P_m e^{-i\mathscr{k}_m d} B_m - \sum_{m'=-2}^{+\infty} X(\kappa_{m'}, \mathscr{k}_m) \left(e^{-i\kappa_{m'} d} C_{m'} + e^{i\kappa_{m'} d} D_{m'} \right)
$$

$$
- \left\{ \begin{array}{l} \displaystyle\sum_{i=1}^{N_a} \mathcal{F}_m(d, a_i) \alpha_i + \sum_{i=1}^{N_b} \dfrac{\partial^2 \mathcal{F}_m(d, b_i)}{\partial x_0^2} \beta_i \\[4mm] + \displaystyle\sum_{i=1}^{N_c} \left[\dfrac{\partial^3 \mathcal{F}_m(d, c_i)}{\partial x_0^3} \gamma_i + \dfrac{\partial^2 \mathcal{F}_m(d, c_i)}{\partial x_0^2} \mu_i \right] \end{array} \right\} = 0, \quad m = 0, 1, 2\ldots, \tag{35b}
$$

07 March 2024 13:22:56

where

$$
\begin{cases}
X(x_1, x_2) = \displaystyle\int_{-H}^{0} \frac{\cosh x_1(z+H)}{\cosh x_1 H} \frac{\cosh x_2(z+H)}{\cosh x_2 H} dz = \begin{cases} \dfrac{x_1 \tanh x_1 H - x_2 \tanh x_2 H}{x_1^2 - x_2^2} & x_1 \neq x_2, \\[2ex] \dfrac{\sinh 2x_1 H + 2x_1 H}{4x_1 \cosh^2 x_1 H} & x_1 = x_2 \end{cases} & \text{(36a)} \\[6ex]
P_m = X(\mathcal{k}_m, \mathcal{k}_m) = \dfrac{2\mathcal{k}_m H + \sinh(2\mathcal{k}_m H)}{4\mathcal{k}_m \cosh^2(\mathcal{k}_m H)}, & \text{(36b)} \\[3ex]
\mathcal{F}_m(x, x_0) = \displaystyle\int_{-H}^{0} \mathcal{G}(x, z, x_0)\varphi_m(z) = \pi i \sum_{m'=-2}^{+\infty} \dfrac{X(\kappa_{m'}, \mathcal{k}_m)\tanh(\kappa_{m'}H)e^{-i\kappa_{m'}|x-x_0|}}{Q_{m'}}. & \text{(36c)}
\end{cases}
$$

To match the velocity at $x = \pm d$, we may apply

$$
\left\langle \frac{\partial \phi^{(2)}(\pm d, z)}{\partial x}, \psi_m(z) \right\rangle = \int_{-H}^{0} \frac{\partial \phi^{(2)}(\pm d, z)}{\partial x} \psi_m(z) dz + \frac{L}{\rho\omega^2}\left[\frac{\partial^2 \phi^{(2)}(\pm d, 0)}{\partial x \partial z} \frac{d^3 \psi_m(0)}{dz^3} + \frac{\partial^4 \phi^{(2)}(\pm d, 0)}{\partial x \partial z^3} \frac{d.\psi_m(0)}{dz} \right]. \tag{37}
$$

Equations (33b) and (33d) give

$$
\begin{cases}
\left\langle \dfrac{\partial \phi^{(2)}(-d, z)}{\partial x}, \psi_m(z) \right\rangle = \displaystyle\int_{-H}^{0} \dfrac{\partial \phi^{(1)}(-d, z)}{\partial x} \psi_m(z) dz + \dfrac{L}{\rho\omega^2}\left[\dfrac{\partial^2 \phi^{(2)}(-d, 0)}{\partial x \partial z} \dfrac{d^3 \psi_m(0)}{dz^3} + \dfrac{\partial^4 \phi^{(2)}(-d, 0)}{\partial x \partial z^3} \dfrac{d\psi_m(0)}{dz} \right], & \text{(38a)} \\[3ex]
\left\langle \dfrac{\partial \phi^{(2)}(d, z)}{\partial x}, \psi_m(z) \right\rangle = \displaystyle\int_{-H}^{0} \dfrac{\partial \phi^{(3)}(d, z)}{\partial x} \psi_m(z) dz + \dfrac{L}{\rho\omega^2}\left[\dfrac{\partial^2 \phi^{(2)}(d, 0)}{\partial x \partial z} \dfrac{d^3 \psi_m(0)}{dz^3} + \dfrac{\partial^4 \phi^{(2)}(d, 0)}{\partial x \partial z^3} \dfrac{d\psi_m(0)}{dz} \right]. & \text{(38b)}
\end{cases}
$$

We may further define

$$
\begin{cases}
\dfrac{\partial^2 \phi^{(2)}(\pm d, 0)}{\partial x \partial z} = \zeta_\pm, & \text{(39a)} \\[3ex]
\dfrac{\partial^4 \phi^{(2)}(\pm d, 0)}{\partial x \partial z^3} = \xi_\pm, & \text{(39b)}
\end{cases}
$$

where $\zeta_\pm$ and $\xi_\pm$ are introduced as additional unknowns to satisfy the edge conditions at $x = \pm d$ later. Substituting Eqs. (11), (12), (13), (16), and (32) into Eqs. (38a) and (38b), as well as using the orthogonality of $\psi_m(z)$, which provides

$$
-i\sum_{m'=0}^{+\infty} X(\kappa_m, \mathcal{k}_{m'})\mathcal{k}_{m'}e^{-i\mathcal{k}_{m'}d}A_{m'} + i\kappa_m Q_m\left(-e^{i\kappa_m d}C_m + e^{-i\kappa_m d}D_m\right)
$$
$$
+ \left\{ \begin{array}{l} \displaystyle\sum_{i=1}^{N_a} \frac{\partial g_m(-d, a_i)}{\partial x}\alpha_i + \sum_{i=1}^{N_b} \frac{\partial^3 g_m(-d, b_i)}{\partial x \partial x_0^2}\beta_i \\[2ex] + \displaystyle\sum_{i=1}^{N_c}\left[\frac{\partial^4 g_m(-d, c_i)}{\partial x \partial x_0^3}\gamma_i + \frac{\partial^3 g_m(-d, c_i)}{\partial x \partial x_0^2}\mu_i \right] \end{array} \right\} + \kappa_m \tanh(\kappa_m H)\left(\kappa_m^2 \zeta_- + \xi_-\right) = -iX(\kappa_m, \mathcal{k}_0)\mathcal{k}_0 I e^{i\mathcal{k}_0 d}, \quad m = -2, -1, 0, 1 \ldots, \tag{40a}
$$

$$
i\sum_{m'=0}^{+\infty} X(\kappa_m, \mathcal{k}_{m'})\mathcal{k}_{m'}e^{-i\mathcal{k}_{m'}d}B_{m'} + i\kappa_m Q_m\left(-e^{-i\kappa_m d}C_m + e^{i\kappa_m d}D_m\right)
$$
$$
+ \left\{ \begin{array}{l} \displaystyle\sum_{i=1}^{N_a} \frac{\partial g_m(d, a_i)}{\partial x}\alpha_i + \sum_{i=1}^{N_b} \frac{\partial^3 g_m(d, b_i)}{\partial x \partial x_0^2}\beta_i \\[2ex] + \displaystyle\sum_{i=1}^{N_c}\left[\frac{\partial^4 g_m(d, c_i)}{\partial x \partial x_0^3}\gamma_i + \frac{\partial^3 g_m(d, c_i)}{\partial x \partial x_0^2}\mu_i \right] \end{array} \right\} + \kappa_m \tanh(\kappa_m H)\left(\kappa_m^2 \zeta_+ + \xi_+\right) = 0, \quad m = -2, -1, 0 \ldots, \tag{40b}
$$

where

$$
g_m(x, x_0) = \left\langle \mathcal{G}(x, z, x_0), \psi_m(z) \right\rangle = \pi i \tanh(\kappa_m H)e^{-i\kappa_m|x-x_0|}. \tag{41}
$$

The remaining equations can be established from the edge conditions at $x = a_j, b_j, c_j$, and $x = \pm d$. In particular, applying Eq. (7a) to Eq. (32), the edge condition at $x = a_j$ ($j = 1 \sim N_a$) gives

07 March 2024 13:22:56

$$\sum_{m'=-2}^{+\infty} \left[f_m^-(a_j) C_{m'} + f_{m'}^+(a_j) D_{m'} \right] + \left\{ \begin{array}{l} \sum_{i=1}^{N_a} \mathcal{W}(a_j, a_i)\alpha_i + \sum_{i=1}^{N_b} \frac{\partial^2 \mathcal{W}(a_j, b_i)}{\partial x_0^2}\beta_i \\ + \sum_{i=1}^{N_c} \left[\frac{\partial^3 \mathcal{W}(a_j, c_i)}{\partial x_0^3}\gamma_i + \frac{\partial^2 \mathcal{W}(a_j, c_i)}{\partial x_0^2}\mu_i \right] \end{array} \right\} = 0, \tag{42}$$

where

$$\begin{cases} f_m^\pm(x) = \kappa_m \tanh(\kappa_m H) e^{\pm i\kappa_m x}, & \text{(43a)} \\ \\ W(x, x_0) = \dfrac{\partial \mathcal{G}(x, 0, x_0)}{\partial z} = \pi i \sum_{m=-2}^{+\infty} \dfrac{\kappa_m \tanh^2(\kappa_m H) e^{-i\kappa_m|x-x_0|}}{Q_m}. & \text{(43b)} \end{cases}$$

Applying Eq. (8b) to Eq. (32), the edge condition at $x = b_j$ ($j = 1 \sim N_b$) gives

$$\sum_{m'=-2}^{+\infty} \left[\frac{d^2 f_{m'}^-(b_j)}{dx^2} C_{m'} + \frac{d^2 f_{m'}^+(b_j)}{dx^2} D_{m'} \right] + \left\{ \begin{array}{l} \sum_{i=1}^{N_a} \frac{\partial^2 \mathcal{W}(b_j, a_i)}{\partial x^2}\alpha_i + \sum_{i=1}^{N_b} \frac{\partial^4 \mathcal{W}(b_j, b_i)}{\partial x^2 \partial x_0^2}\beta_i \\ + \sum_{i=1}^{N_c} \left[\frac{\partial^5 \mathcal{W}(b_j, c_i)}{\partial x^2 \partial x_0^3}\gamma_i + \frac{\partial^4 \mathcal{W}(b_j, c_i)}{\partial x^2 \partial x_0^2}\mu_i \right] \end{array} \right\} = 0. \tag{44}$$

Using Eqs. (9a) and (9b) to Eq. (32), the edge condition at $x = c_j$ ($j = 1 \sim N_b$) gives

$$\sum_{m'=-2}^{+\infty} \left[\frac{d^2 f_{m'}^-(c_j)}{dx^2} C_{m'} + \frac{d^2 f_{m'}^+(c_j)}{dx^2} D_{m'} \right] + \left\{ \begin{array}{l} \sum_{i=1}^{N_a} \frac{\partial^2 \mathcal{W}(c_j, a_i)}{\partial x^2}\alpha_i + \sum_{i=1}^{N_b} \frac{\partial^4 \mathcal{W}(c_j, b_i)}{\partial x^2 \partial x_0^2}\beta_i \\ + \sum_{i=1}^{N_c} \left[\frac{\partial^5 \mathcal{W}(c_j, c_i)}{\partial x^2 \partial x_0^3}\gamma_i + \frac{\partial^4 \mathcal{W}(c_j, c_i)}{\partial x^2 \partial x_0^2}\mu_i \right] \end{array} \right\} = 0, \tag{45a}$$

$$\sum_{m'=-2}^{+\infty} \left[\frac{d^3 f_{m'}^-(c_j)}{dx^3} C_{m'} + \frac{d^3 f_{m'}^+(c_j)}{dx^3} D_{m'} \right] + \left\{ \begin{array}{l} \sum_{i=1}^{N_a} \frac{\partial^3 \mathcal{W}(c_j, a_i)}{\partial x^3}\alpha_i + \sum_{i=1}^{N_b} \frac{\partial^5 \mathcal{W}(b_j, b_i)}{\partial x^3 \partial x_0^2}\beta_i \\ + \sum_{i=1}^{N_c} \left[\frac{\partial^6 \mathcal{W}(c_j, c_i)}{\partial x^3 \partial x_0^3}\gamma_i + \frac{\partial^5 \mathcal{W}(c_j, c_i)}{\partial x^3 \partial x_0^2}\mu_i \right] \end{array} \right\} = 0. \tag{45b}$$

If the edges at $x = \pm d$ are free to move, substituting Eq. (32) into Eq. (6a), similar equations shown in Eqs. (45a) and (45b) need to be satisfied, or

$$\sum_{m'=-2}^{+\infty} \left[\frac{d^2 f_{m'}^-(\pm d)}{dx^2} C_{m'} + \frac{d^2 f_{m'}^+(\pm d)}{dx^2} D_{m'} \right] + \left\{ \begin{array}{l} \sum_{i=1}^{N_a} \frac{\partial^2 \mathcal{W}(\pm d, a_i)}{\partial x^2}\alpha_i + \sum_{i=1}^{N_b} \frac{\partial^4 \mathcal{W}(\pm d, b_i)}{\partial x^2 \partial x_0^2}\beta_i \\ + \sum_{i=1}^{N_c} \left[\frac{\partial^5 \mathcal{W}(\pm d, c_i)}{\partial x^2 \partial x_0^3}\gamma_i + \frac{\partial^4 \mathcal{W}(\pm d, c_i)}{\partial x^2 \partial x_0^2}\mu_i \right] \end{array} \right\} = 0, \tag{46a}$$

$$\sum_{m'=-2}^{+\infty} \left[\frac{d^3 f_{m'}^-(\pm d)}{dx^3} C_{m'} + \frac{d^3 f_{m'}^+(\pm d)}{dx^3} D_{m'} \right] + \left\{ \begin{array}{l} \sum_{i=1}^{N_a} \frac{\partial^3 \mathcal{W}(\pm d, a_i)}{\partial x^3}\alpha_i + \sum_{i=1}^{N_b} \frac{\partial^5 \mathcal{W}(\pm d, b_i)}{\partial x^3 \partial x_0^2}\beta_i \\ + \sum_{i=1}^{N_c} \left[\frac{\partial^6 \mathcal{W}(c_j, c_i)}{\partial x^3 \partial x_0^3}\gamma_i + \frac{\partial^5 \mathcal{W}(\pm d, c_i)}{\partial x^3 \partial x_0^2}\mu_i \right] \end{array} \right\} = 0. \tag{46b}$$

By contrast, if the edges at $x = \pm d$ are pinned to the seabed, the zero-shear force condition in Eq. (46b) should be replaced by the zero-deflection condition as

$$\sum_{m'=-2}^{+\infty} \left[f_{m'}^-(\pm d) C_{m'} + f_{m'}^+(\pm d) D_{m'} \right] + \left\{ \begin{array}{l} \sum_{i=1}^{N_a} \mathcal{W}(\pm d, a_i)\alpha_i + \sum_{i=1}^{N_b} \frac{\partial^2 \mathcal{W}(\pm d, b_i)}{\partial x_0^2}\beta_i \\ + \sum_{i=1}^{N_c} \left[\frac{\partial^3 \mathcal{W}(\pm d, c_i)}{\partial x_0^3}\gamma_i + \frac{\partial^2 \mathcal{W}(\pm d, c_i)}{\partial x_0^2}\mu_i \right] \end{array} \right\} = 0. \tag{47}$$
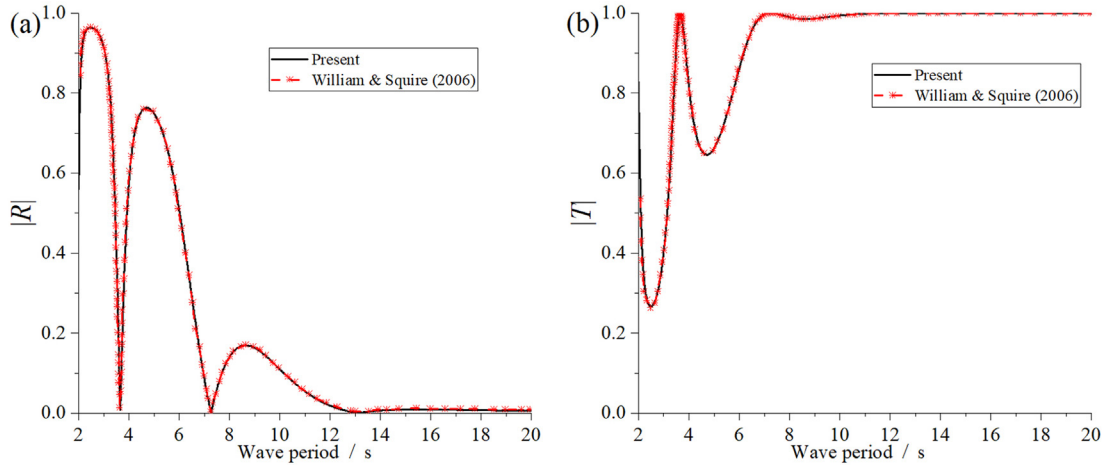
FIG. 2. The reflection and transmission coefficients for an incident wave diffracted by a single floating elastic plate: (a) reflection coefficients; (b) transmission coefficients.

If the infinite series in Eqs. (13), (16), and (31) are truncated at $m = M$, there will be $M + 1$ unknowns for A_m, $M + 1$ for B_m, $M + 3$ for C_m, and $M + 3$ for D_m. In addition, the edge condition at $x = a_i \, (i = 1 \sim N_a)$ provides N_a unknowns for α_i. The edge condition at $x = b_i \, (i = 1 \sim N_b)$ gives N_b unknowns for β_i. The edge condition at $x = c_i \, (i = 1 \sim N_c)$ gives $2N_c$ unknowns for γ_i and μ_i, respectively. The edge conditions at $x = \pm d$ also provide four additional unknowns for $\zeta_\pm$ and $\xi_\pm$, respectively. In such a case, we have $4M + 12 + N_a + N_b + 2N_c$ unknowns. Equations (35a), (35b), (40a), and 40(b) provide $4M + 8$ equations, and Eqs. (42) and (44)–(47) offer $N_a + N_b + 2N_c + 4$ equations. Hence, the total number of unknowns is equal to the total number of equations, and all the unknowns can be fully solved. By contrast, if we employ the procedure of MEE in Ren, et al.[13] instead, there will be a total of $2(M + 1) + 2(N_a + N_b + N_c + 1)(M + 3)$ unknown coefficients to solve. It can be found that the number of unknowns is significantly reduced by using the present method.

IV. RESULTS AND DISCUSSION

The typical values of physical parameters of an elastic plate are selected based on the data in Xia et al.,[27]

$$L = 1.96 \times 10^{11}\,\mathrm{N \cdot m}, \quad \rho_e = 1000\,\mathrm{kg/m^3}, \quad h_e = 5\,\mathrm{m}, \quad d = 150\,\mathrm{m}. \tag{48}$$

Other parameters are chosen as $\rho = 1025\,\mathrm{kg/m^3}$, $g = 9.81\,\mathrm{m/s^2}$, and $H = 50\,\mathrm{m}$. Those parameters outlined above will be applied in subsequent computations unless specified otherwise. The infinite series in Eqs. (13), (16), and (31) are truncated at $m = M = 100$, which has been confirmed to be convergent.

A. Validation of the method

Let $|x| \to +\infty$ in the velocity potential in Eqs. (11), (12), (13), and (16), all the decay terms will be zero, and we have

$$\phi(x, z) = \begin{cases} I(Re^{ik_0 x} + e^{-ik_0 x})\varphi_0(z) & x \to -\infty \\ IT\varphi_0(z)e^{-ik_0 x} & x \to +\infty \end{cases}, \tag{49}$$

where $R = A_0/I$ and $T = B_0/I$ denote the reflection and transmission coefficients, respectively. The approach applied here is validated by comparing with the results of $|R|$ and $|T|$ in Williams and Squire[10] for water wave diffracted by a single floating ice cover in deep water, which was solved via the Wiener–Hopf technique.[28] $|R|$ and $|T|$ vs the wave period are plotted in Fig. 2, and a very good consistency can be observed.

In the following sections, all the numerical results will be presented in nondimensionalized forms, based on the water density ρ, acceleration due to gravity g, and the mean water depth H. $\tau = \mathcal{T}\sqrt{g/H}$ is used to represent the dimensionless wave period $\mathcal{T}$, where $\mathcal{T} = 2\pi/\omega$. Similar with Williams and Squire,[10] we may display the results of $\tau > 1$ here, and much attention is paid to long waves.

B. Wave interaction with floating elastic plates with same type of internal constraints

In this section, all the internal edges of the plates are considered as a single type, namely, pinned, hinged, or free. For each type of edge, we aim to understand how the number of edges affects the reflected and transmitted waves at the far-field, as well as the deflection and strain in the elastic plates. Notably, the waves at infinity can be used to assess the environmental impact of deploying solar panels at sea. The deflection and strain provide insights into the hydroelastic response of solar panels to ocean waves.

1. All internal constraints are pinned supports

The pinned supports are assumed to be distributed uniformly along the plate, which gives

$$a_i = -d + \frac{2d}{N_a + 1}i, \quad i = 1 \sim N_a, \tag{50}$$

where a_i is defined in Table I. The results of reflection and transmission coefficients are shown in Fig. 3. It should be noted that when τ is small (corresponding to short waves), very highly rapid changes on $|T|$ and $|R|$ are expected,[10,16] which is not included in the figures. On the
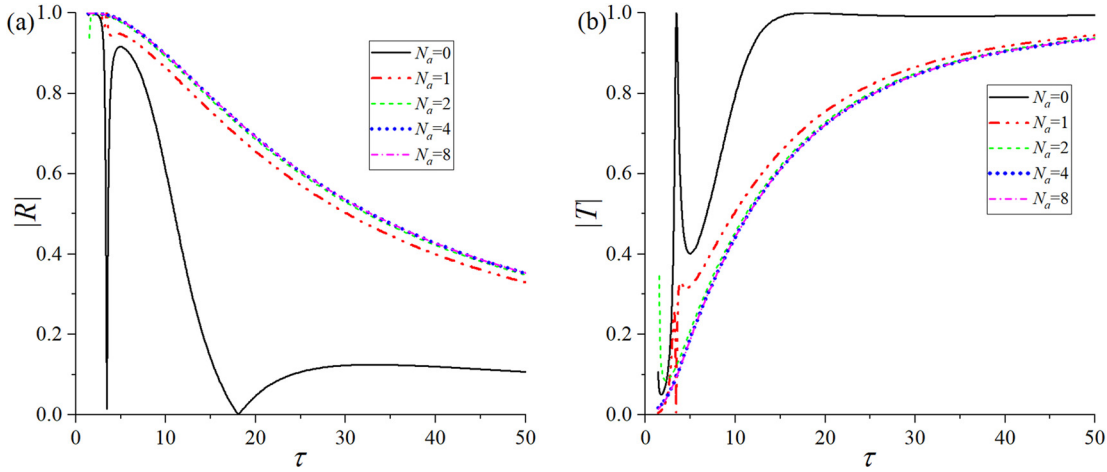
FIG. 3. The reflection and transmission coefficients vs the wave period under different numbers of internal pinned supports: (a) reflection coefficients; (b) transmission coefficients. Here, two edges at $x = \pm d$ are pinned, $N_b = N_c = 0$.

curve of $N_a = 0$, T first decreases to a very small value as τ increases and then quickly increases to a peak value around $\tau \approx 4.88$. As τ continues to increase, $|R|$ decreases to a value close to 0, and then, $|R|$ increases and varies much more slowly. When there is a pined support in the elastic plate ($N_a = 1$), the result becomes quite different. Specifically, $|R|$ ($|T|$) generally decreases (increases) as τ increases within the range considered in Fig. 3. In addition, at a fixed value of τ, if more pinned points are imposed on the plate, there will first be a slight increase (decrease) in $|R|$ ($|T|$). However, as N_a increases, the curves of $|R|$ ($|T|$) under $N_a = 4$ and 8 are nearly identical, which means the effect of N_a on $|R|$ ($|T|$) becomes quite weak after $N_a \geq 4$. In fact, more pinned supports in the structure means more 0-deflection points on the plate. When N_a is sufficiently large, the floating elastic plate will behave similarly to a rigid plate. Furthermore, from the aspect of wave energy, when pinned supports are imposed on the plate. For long waves, compared with the panel without any pin, the wave energy on reflected waves will increase and the on transmitted waves will decrease.

The deflection η and principal strain ε of the elastic plate are also considered, which can be calculated from[29]

$$\begin{cases} \eta(x) = \dfrac{1}{i\omega}\dfrac{\partial \phi^{(2)}(x,0)}{\partial z}, & \text{(51a)} \\[2mm] \varepsilon(x) = \dfrac{h_e}{2}\left|\dfrac{d^2\eta(x)}{dx^2}\right|. & \text{(51b)} \end{cases}$$

Substituting Eq. (32) into (51a), $\eta(x)$ gives

$$\eta(x) = \frac{1}{i\omega}\sum_{m=-2}^{+\infty}\left[C_m f_m^-(x) + D_m f_m^+(x)\right]$$

$$+ \frac{1}{i\omega}\left\{ \begin{aligned} &\sum_{i=1}^{N_a}\alpha_i \mathcal{W}(x,a_i) + \sum_{i=1}^{N_b}\beta_i\frac{\partial^2\mathcal{W}(x,b_i)}{\partial x_0^2} \\ &+ \sum_{i=1}^{N_c}\left[\gamma_i\frac{\partial^3\mathcal{W}(x,c_i)}{\partial x_0^3} + \mu_i\frac{\partial^2\mathcal{W}(x,c_i)}{\partial x_0^2}\right] \end{aligned}\right\}. \quad \text{(52)}$$

We may define $\eta_{max} = \max_{-d\leq x\leq d}|\eta(x)|$ as the maximum plate deflection and $\varepsilon_{max} = \max_{-d\leq x\leq d}\varepsilon(x)$ as the maximum principal strain. η_{max}/A and $\varepsilon_{max}H/A$ vs the wave period τ are given in Fig. 4. In Fig. 4(a), when $N_a = 0$, η_{max}/A initially increases with τ, and reaching a peak $\eta_{max}/A \approx 1.085$ at $\tau \approx 18.4$. Subsequently, it gradually declines and approaches 1. By contrast, when an internal pin is added ($N_a = 1$), in addition to the region near the peaks of η_{max}/A, it can be found that η_{max}/A becomes much smaller in most range of τ. As N_a becomes larger, η_{max}/A further declines. When $N_a \geq 4$, η_{max}/A can even be close to zero. In Fig. 4(b), $\varepsilon_{max}H/A$ at $N_a = 1$ is normally greater than that at $N_a = 0$. However, when $N_a \geq 2$, the strain level becomes smaller than that without any pin. In addition, $\varepsilon_{max}H/A$ is further declined as N_a further increases.

2. All internal constraints are hinged supports

We may also consider the scenario floating elastic panels connected by internal hinges ($N_a = N_c = 0$), where the positions b_i ($i = 1 \sim N_b$) of the internal hinges are assumed to present in the same distribution as the pins in Eq. (50), and two side edges at $x = \pm d$ are set to be free. The results of the reflection and transmission coefficients are given in Fig. 5. It can be observed that as N_b increases, the curves of $|R|$ and $|T|$ are significantly changed, which indicates that $|R|$ and $|T|$ are quite sensitive to N_b. Typically, at $N_b = 4$, a local oscillation of $|R|$ vs τ is observed, and such behavior becomes much more evident at $N_b = 8$, as shown in the local enlargement in Fig. 5(a). The results of the maximum deflection and principal strain of the elastic plate are presented in Fig. 6. In Fig. 6(a), η_{max}/A at each N_b generally shows a similar variation trend. In particular, η_{max}/A first increases with τ, and peaks at $\tau = 10.80, 6.50, 5.30, 4.26,$ and 3.46 with $\eta_{max}/A = 1.34, 1.99, 2.54, 3.28,$ and 4.28 for $N_b = 0, 1, 2, 4, 8$, respectively. Subsequently, η_{max}/A gradually decreases and approaches 1 with the increase in τ. Notably, there is a positive correlation between the spike value and N_b. In Fig. 6(b), the introduction of additional hinged supports on the plate generally leads to a decrease in $\varepsilon_{max}H/A$. To clearly illustrate the behavior of plate deflection at the spikes depicted in Fig. 6(a), the corresponding $|\eta(x)|$ vs x/d is plotted in Fig. 7. It can be
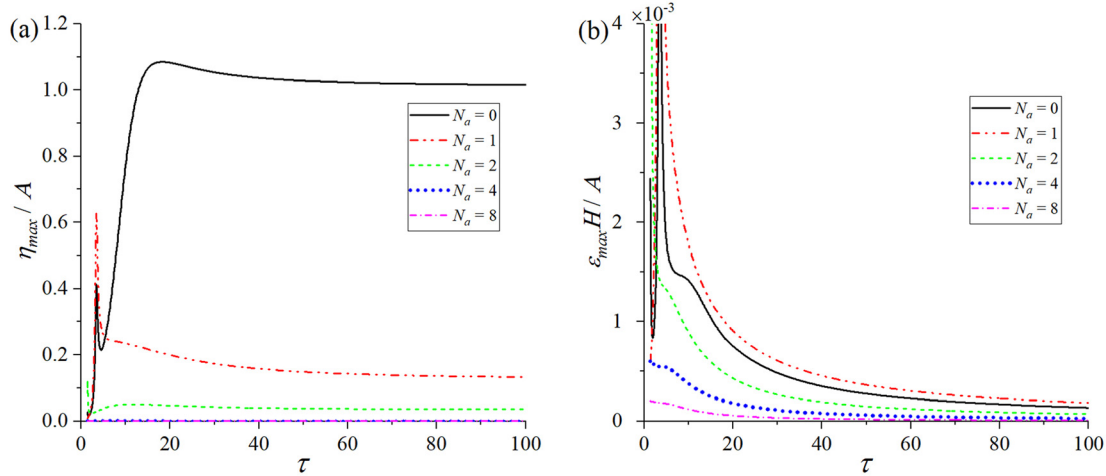
FIG. 4. The maximum deflection and principal strain in the elastic plate vs the wave period under different numbers of internal pinned supports: (a) maximum deflection; (b) maximum principal strain. Here, two edges at $x = \pm d$ are pinned, $N_b = N_c = 0$.
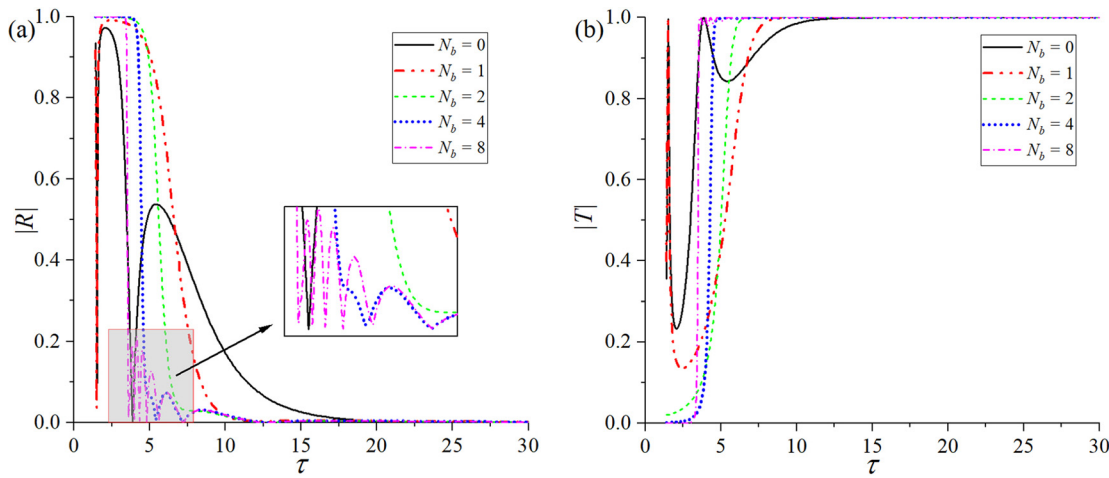

FIG. 5. The reflection and transmission coefficients vs the wave period under different numbers of internal hinges: (a) reflection coefficients; (b) transmission coefficients. Here, two edges at $x = \pm d$ are free, $N_a = N_c = 0$.

observed that η_{max} in all the cases are occurred at $x = -d$. The profiles of $|\eta(x)|/A$ exhibit a degree of similarity across different values of N_b. In particular, $|\eta(x)|/A$ shows alternating variation with x/d with N_b troughs and $N_b + 2$ peaks. These peaks are located at the edges of each panel, and the corresponding peak values decrease as x/d. Moreover, at $N_b = 1$, obvious bending is observed in both *two* panels. However, as N_b increases, the bending in each plate is unobvious, and the entire structure performs like a series of rigid plates, which indicates that the elasticity of the structure becomes less important.

3. All internal constraints are free

Wave diffraction by multiple floating elastic panels without any connection is also considered ($N_a = N_b = 0$). The reflection and transmission coefficients are presented in Fig. 8. Similar with the phenomenon observed in Fig. 5, it can be found that $|R|$ and $|T|$ are also very sensitive to the number of internal free edges N_c. As N_c increases, local oscillations on $|R|$ and $|T|$ vs τ are also observed, such phenomenon is consistent with the results for an elastic plate of infinite extent with multiple cracks.[30] Compared with Fig. 5 for plates connected with hinges, the local oscillation here is much stronger. In fact, such local oscillatory behavior is due to the multiple reflections of the traveling waves between two edges of the plate. With less restriction on the edge conditions, the energy conversion between waves and plate motion is much more flexible and may be sensitive to the properties of ocean waves. Such conversion results in rapid variations of the energy in the corresponding radiated and diffracted waves, thereby leading to more pronounced oscillation phenomena. Consequently, in scenarios of free
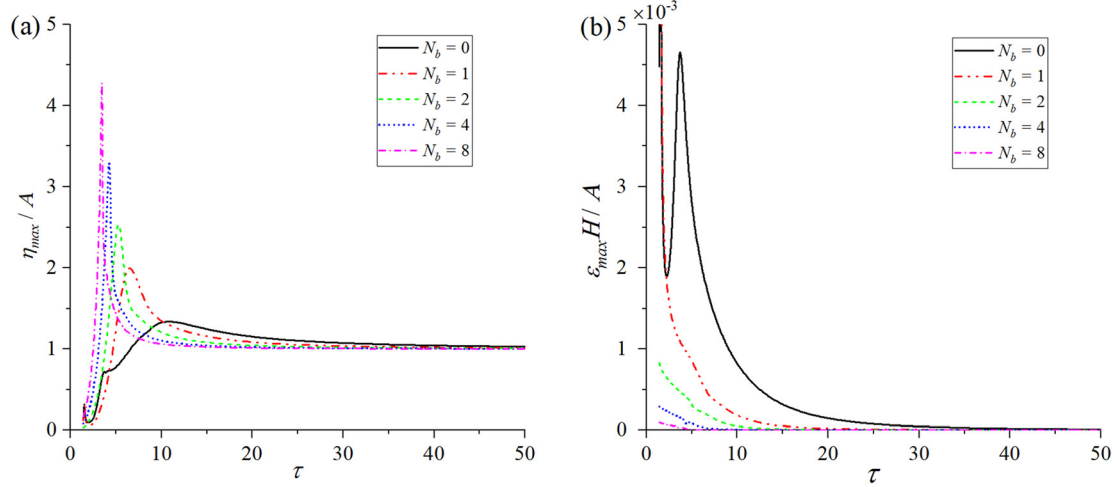
FIG. 6. The maximum deflection and principal strain in the elastic plates connected by one or multiple internal hinges: (a) maximum deflection; (b) maximum principal strain. Here, two edges at $x = \pm d$ are free, $N_a = N_c = 0$.
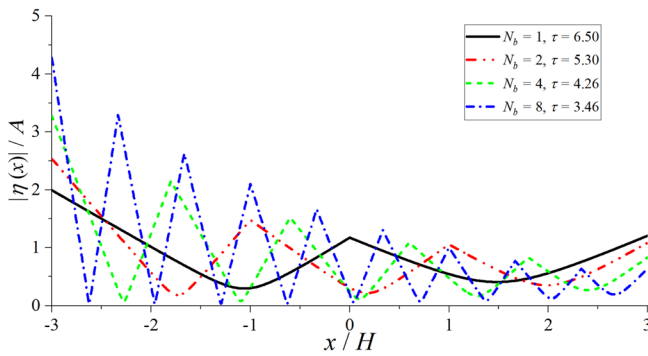

FIG. 7. Deflection of the elastic plate. Here, two edges at $x = \pm d$ are free, $N_a = N_c = 0$.

edges, more evident oscillatory behavior in terms of reflection and transmission coefficients is expected. In Fig. 9(a), obvious spikes can be observed in the curves of η_{max}/A vs τ, and these peak values increase with N_c, which is similar with the phenomenon in Fig. 6(a). However, there is also a highly local oscillation near the peak, a feature that markedly diverges from that in Fig. 6(a). $\varepsilon_{max}H/A$ in Fig. 9(b) generally decreases with N_c at a fixed τ. In addition, a weak local oscillation is also observed in $\varepsilon_{max}H/A$ vs τ as N_c increases.

C. Wave interaction with floating elastic plates with different type of internal constraints

In actual engineering structures, each of the panel components can be designed to be connected by certain edge conditions, and mooring lines are usually used to improve the stability of the entire structure.
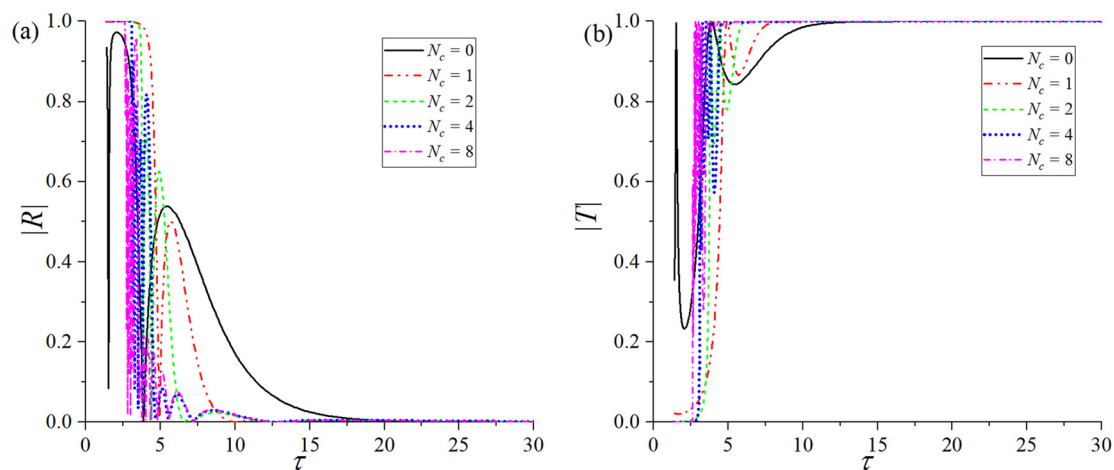

FIG. 8. The reflection and transmission coefficients vs the wave period under different numbers of internal free edges: (a) reflection coefficients; (b) transmission coefficients. Here, two edges at $x = \pm d$ are free, $N_a = N_b = 0$.
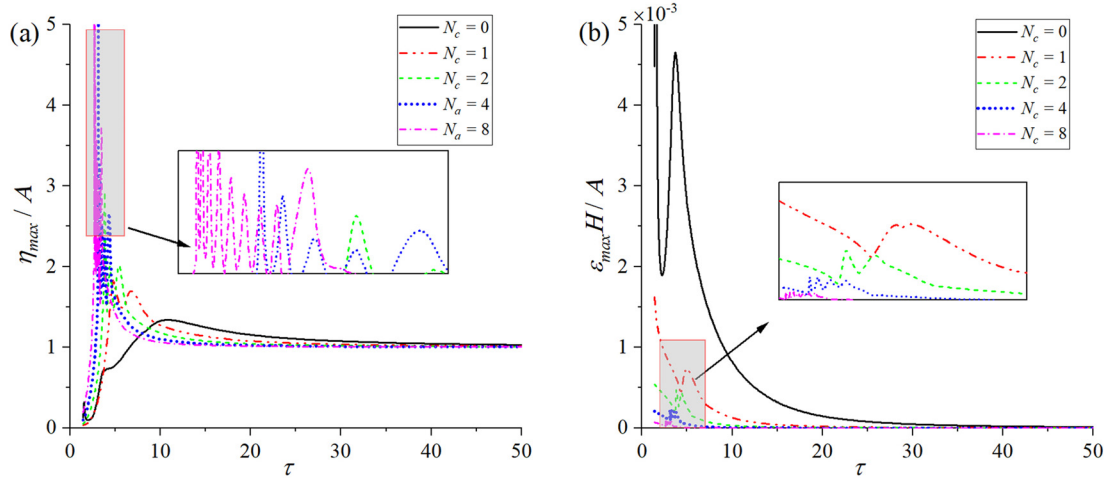
FIG. 9. The maximum deflection and principal strain in the elastic plates with free edge conditions: (a) maximum deflection; (b) maximum principal strain. Here, two edges at $x = \pm d$ are free, $N_a = N_b = 0$.

Hence, considering the combined effects of various types of physical constraints on the hydrodynamic properties of the structure is quite necessary. Here, we may consider a scenario that three identical elastic plates are connected by two hinges ($b_1 = -d/3$, $b_2 = d/3$), and we try to arrange pinned supports on these plates to reduce the maximum deflection and principal strain in the structure, which can be regarded as a theoretical study to optimize the mooring positions for a series of hinged floating elastic plates. Here, four different configurations are considered, as shown in Fig. 10. The corresponding results are given in Fig. 11. In Fig. 11(a), if only one pinned support is imposed at $x = 0$ [Fig. 10 (a)], compared with the case without any pin, η_{max}/A becomes even much larger over a wide range of τ, which is different from the result for a single plate in Fig. 4(a). By contrast, Fig. 11(a) also indicated that the other three configurations in Fig. 10 can effectively mitigate the magnitude of η_{max}/A. In particular, apart from some narrow peaks

in η_{max}/A when τ is small, the configuration in Fig. 10(d) emerges as the most effective, followed by the configuration in Fig. 10(b) and, subsequently, Fig. 10(c). For the maximum principal strain on the plate given in Fig. 11(b), it is observed that every configuration in Fig. 10 results in an increase in $\varepsilon_{max}H/A$, across a wide range of τ, compared to the scenario without any pinned support. However, the increase is relatively less under the configurations presented in Figs. 10(b) and 10(d). Furthermore, Fig. 11(b) reveals a marked and rapid variation in $\varepsilon_{max}H/A$ within the range of $5.35 \leq \tau \leq 5.55$ under the configuration in Fig. 10(b), and it is associated with the spike on η_{max}/A in Fig. 11(a). Correspondingly, this phenomenon is also reflected in the deflection and principal strain distributions in the plate, as illustrated in Fig. 12. In addition, we also observe that η_{max}/A is maximum at $x = \pm d$ and $x = \pm d/2$ with a close value, and $\varepsilon_{max}H/A$ is maximum at the pinned positions at $x = \pm 2d/3$.
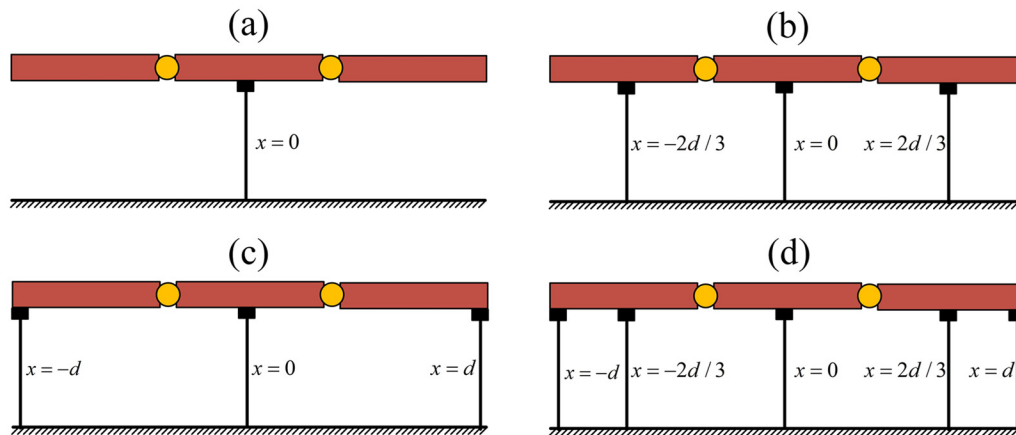

FIG. 10. Four different schemes to arrange pinned supports. (a) $a_1 = 0$; (b) $a_1 = -\frac{2d}{3}$, $a_2 = 0$, $a_3 = \frac{2d}{3}$; (c) $a_1 = -d$, $a_2 = 0$, $a_3 = d$; (d) $a_1 = -d$, $a_2 = -\frac{2d}{3}$, $a_3 = 0$, $a_4 = \frac{2d}{3}$, $a_5 = d$.
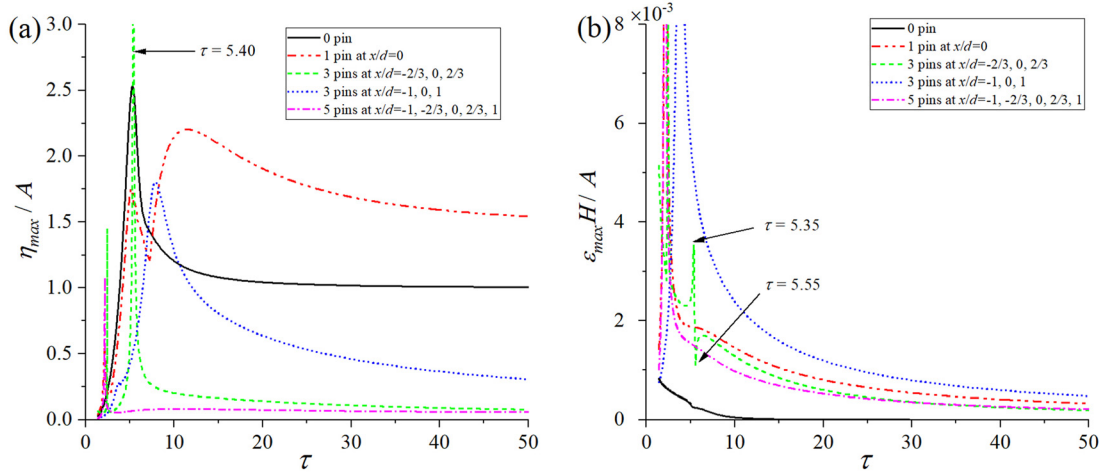
FIG. 11. The maximum deflection (a) and principal strain (b) in the elastic plates corresponding to the configurations in Fig. 10.
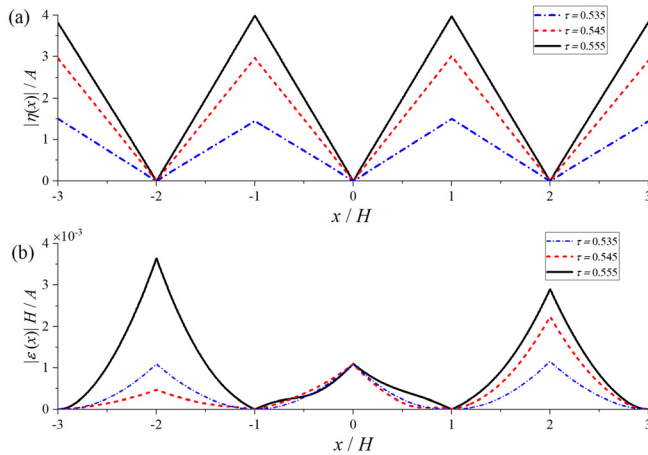

FIG. 12. Deflection (a) and distribution of the principal strain (b) of the elastic plate. Two edges at $x = \pm d$ are free, $N_a = 3$ with $a_1 = -\frac{2d}{3}$, $a_2 = 0$, $a_3 = \frac{2d}{3}$, $N_b = 2$ with $b_1 = -\frac{d}{3}$, $b_2 = \frac{d}{3}$, $N_c = 0$.

V. CONCLUSION

The problem of wave interaction with multiple adjacent floating solar panels with three different types of constraints is considered, namely, pinned, hinged, and free. The solution procedure is based on a domain decomposition methodology, where the velocity potential of the fluid beneath the solar panels is constructed through the boundary integral equation by invoking the Green function for fluid fully covered by an elastic plate. The velocity potential in the free surface domain is expanded as a conventional infinite series by using vertical mode expansion. Such an approach makes the computation much more effective, since the unknown coefficients only need to be distributed on two interfaces, as well as the jumps of physical parameters of the plates.

Based on the developed scheme, the effects of three constraints on the elastic plates are extensively investigated. It is found that pinned supports can increase (decrease) the reflection coefficient $|R|$ (transmission coefficient $|T|$) for long waves. With the number of pinned supports increases, the magnitude of maximum deflection η_{max} and principal strain ε_{max} in the plates can be reduced. For multiple adjacent floating elastic panels connected by hinges or free to each other, it is observed that $|R|$ and $|T|$ are quite sensitive to the number of edges. In addition, a local oscillation will be apparent in the curves of $|R|$ and $|T|$ vs wave period τ, and such a phenomenon is much more evident in the case of free edges. This local oscillation can be attributed to the lesser restriction at the free edges of the plates, resulting in a stronger energy conversion between transmitted and radiated waves. Furthermore, with the increase in the number of edges, spikes in the curve of η_{max} vs τ become more pronounced, as well as ε_{max} is generally decreased.

The combined influence of hinged and pinned supports on the hydrodynamic response of multiple floating elastic plates is also evaluated. A case study is conducted for three identical elastic plates connected by hinged plates. Four distinct configurations with varying pinned points are considered. The analysis revealed that the placement of pinned supports has a considerable impact on both η_{max} and ε_{max}. In some instances, additional pinned supports even result in an increase in η_{max}. The present investigation provides a theoretical attempt to the optimization of mooring positions on floating solar panels.

Although only three typical edge conditions are considered in the present study, the solution procedure can be easily extended to other types of constraints by changing the jump terms in the boundary integral equation.

07 March 2024 13:22:56

AUTHOR DECLARATIONS
Conflict of Interest

The authors have no conflicts to disclose.

Author Contributions

Yifeng Yang: Conceptualization (equal); Data curation (lead); Formal analysis (lead); Methodology (equal); Software (lead); Validation (equal); Visualization (lead); Writing – original draft (lead). **Kang Ren:** Conceptualization (equal); Formal analysis (equal); Funding acquisition (equal); Methodology (equal); Project administration (equal); Supervision (equal); Writing – original draft (equal); Writing – review & editing (lead). **Binzhen Zhou:** Formal analysis (equal); Project administration (equal); Resources (equal); Supervision (equal); Writing – review & editing (equal). **Shi Yan Sun:** Data curation (equal); Funding acquisition (equal); Methodology (equal); Project administration (equal); Supervision (equal); Writing – original draft (equal); Writing – review & editing (equal). **Luofeng Huang:** Conceptualization (equal); Funding acquisition (lead); Project administration (lead); Resources (equal); Supervision (equal); Writing – review & editing (equal).

DATA AVAILABILITY

The data that support the findings of this study are available within the article.

REFERENCES

[1]IRENA, How falling costs make renewables a cost-effective investment (2020).

[2]R. M. Almeida, R. Schmitt, S. M. Grodsky, A. S. Flecker, C. P. Gomes, L. Zhao, H. Liu, N. Barros, R. Kelman, and P. B. McIntyre, "Floating solar power could help fight climate change—Let's get it right," Nature **606**, 246 (2022).

[3]T. Hooper, A. Armstrong, and B. Vlaswinkel, "Environmental impacts and benefits of marine floating solar," Sol. Energy **219**, 11 (2021).

[4]C. Fox and V. A. Squire, "Reflection and transmission characteristics at the edge of shore fast sea ice," J. Geophys. Res. **95**, 11629, https://doi.org/10.1029/JC095iC07p11629 (1990).

[5]N. J. Balmforth and R. V. Craster, "Ocean waves and ice sheets," J. Fluid Mech. **395**, 89 (1999).

[6]M. H. Meylan and V. A. Squire, "The response of ice floes to ocean waves," J. Geophys. Res. **99**, 891, https://doi.org/10.1029/93JC02695 (1994).

[7]C. Wu, E. Watanabe, and T. Utsunomiya, "An eigenfunction expansion-matching method for analyzing the wave-induced responses of an elastic floating plate," Appl. Ocean Res. **17**, 301 (1995).

[8]I. V. Sturova, "Diffraction of surface waves on an inhomogeneous elastic plate," J. Appl. Mech. Tech. Phys. **41**, 612 (2000).

[9]D. V. Evans and R. Porter, "Wave scattering by narrow cracks in ice sheets floating on water of finite depth," J. Fluid Mech. **484**, 143 (2003).

[10]T. D. Williams and V. A. Squire, "Scattering of flexural–gravity waves at the boundaries between three floating sheets with applications," J. Fluid Mech. **569**, 113 (2006).

[11]H. Chung and C. Fox, "Calculation of wave-ice interaction using the Wiener-Hopf technique," New Zealand J. Math **31**, 1 (2002).

[12]Y. Y. Shi, Z. F. Li, and G. X. Wu, "Interaction of wave with multiple wide polynyas," Phys. Fluids **31**, 067111 (2019).

[13]K. Ren, G. X. Wu, and G. A. Thomas, "Wave excited motion of a body floating on water confined between two semi-infinite ice sheets," Phys. Fluids **28**, 127101 (2016).

[14]D. Karmakar and C. G. Soares, "Scattering of gravity waves by a moored finite floating elastic plate," Appl. Ocean Res. **34**, 135 (2012).

[15]S. C. Mohapatra, R. Ghoshal, and T. Sahoo, "Effect of compression on wave diffraction by a floating elastic plate," J. Fluids Struct. **36**, 124 (2013).

[16]D. Karmakar, J. Bhattacharjee, and T. Sahoo, "Wave interaction with multiple articulated floating elastic plates," J. Fluids Struct. **25**, 1065 (2009).

[17]K. M. Praveen, D. Karmakar, and C. Guedes Soares, "Hydroelastic analysis of periodic arrays of multiple articulated floating elastic plate," Ships Offshore Struct. **15**, 280 (2020).

[18]C. W. Zhang, P. F. Wang, L. F. Huang, M. K. Zhang, H. T. Wu, and D. Z. Ning, "Resonance mechanism of hydroelastic response of multi-patch floating photovoltaic structure in water waves over stepped seabed," Phys. Fluids **35**, 107137 (2023).

[19]V. A. Squire, "Of ocean waves and sea-ice revisited," Cold Regions Sci. Technol. **49**, 110 (2007).

[20]V. A. Squire, "Synergies between VLFS hydroelasticity and sea ice research," Int. J. Offshore Polar Eng. **18**, 241–253 (2008).

[21]Y. F. Yang, G. X. Wu, and K. Ren, "Three-dimensional interaction between uniform current and a submerged horizontal cylinder in an ice-covered channel," J. Fluid Mech. **928**, A4 (2021).

[22]K. Ren, G. X. Wu, and Y. F. Yang, "Surface wave interaction with floating elastic plates in channels," Phys. Fluids **36**, 017143 (2024).

[23]R. E. Taylor, "Hydroelastic analysis of plates and some approximations," J. Eng. Math. **58**, 267 (2007).

[24]Z. F. Li, G. X. Wu, and C. Y. Ji, "Wave radiation and diffraction by a circular cylinder submerged below an ice sheet with a crack," J. Fluid Mech. **845**, 682 (2018).

[25]T. Sahoo, T. L. Yip, and A. T. Chwang, "Scattering of surface waves by a semi-infinite floating elastic plate," Phys. Fluids **13**, 3215 (2001).

[26]Y. F. Yang, G. X. Wu, and K. Ren, "Hydroelastic wave diffraction by a vertical circular cylinder standing in a channel with an ice cover," J. Fluid Mech. **941**, A13 (2022).

[27]D. W. Xia, J. W. Kim, and R. C. Ertekin, "On the hydroelastic behavior of two-dimensional articulated plates," Mar. Struct. **13**, 261 (2000).

[28]B. Noble and G. Weiss, "Methods based on the Wiener-Hopf technique for the solution of partial differential equations," Phys. Today **12**(9), 50 (1959).

[29]S. P. Timoshenko and S. Woinowsky-Krieger, *Theory of Plates and Shells* (McGraw-Hill, 1959).

[30]R. Porter and D. V. Evans, "Scattering of flexural waves by multiple narrow cracks in ice sheets floating on water," Wave Motion **43**, 425 (2006).